PAPER

Check for updates

A nontoxic biocompatible nanocomposite comprising black phosphorus with Au–γ-Fe₂O₃ nanoparticles

Atanu Naskar, [ID] [a] Semi Kim [ID] [b] and Kwang-sun Kim [ID] *[a]

Black phosphorus (BP) has emerged as the latest 2D material within the post-graphene scenario, which can be used for various biomedical applications. In this study, we reported a promising nanocomposite material, which could be assembled with Au nanoparticles and γ-Fe₂O₃ nanoparticles on BP nanosheets (AIB), and studied its biocompatibility that promises to be useful for various biomedical applications. The synthesis of the Au–γ-Fe₂O₃ nanomaterial was attained through low-temperature solution synthesis and the exfoliation of BP nanosheets was performed through a liquid ultrasonication process. The individual components were then composited by ultrasonication and stirring. X-ray diffraction and transmission electron microscopic analyses confirmed the existence of Au and γ-Fe₂O₃ nanoparticles (NPs) assembled over BP nanosheets. Moreover, the surface chemical composition and valence state of the elements present in the AIB nanocomposite were evaluated with the help of an X-ray photoelectron spectroscopy study. The AIB nanocomposite exhibited excellent biocompatibility with HCT-15 cells after evaluating through WST assay. Therefore, the excellent biocompatible nature of this BP nanocomposite could be beneficial for various potential biomedical applications.

1. Introduction

Numerous studies based on nanostructured composites have been performed in application-oriented research.[1–3] The main explanation for such extensive research works with nano-structured composites is that they enable researchers to combine materials with different physical and chemical properties in order to expand the range of different applications from one single material. As an example, the combination of magnetic and metallic nanomaterials has been used in applications such as catalysis, biosensing, magnetic resonance imaging, magnetic fluid hyperthermia, and drug delivery.[4–7]

After the immense success of graphene, researchers recently focused on a wide range of thin 2D materials, such as boron nitride, graphite carbon nitride, MXenes, bismuth, zeolitic imidazolate framework (ZIF), different types of carbon based nanoparticles and quantum dots.[8–12] The reasons behind their increasing use for biomedical application can be attributed to their unique physicochemical properties, surface-to-volume ratio, atomic thickness, controllable electronic and mechanical properties.[9] Moreover, they are biologically safe or can be functionalized to make them biocompatible after the

interaction with cell and tissues which makes them ideal for their use in biomedical field.[10]

In the midst of this emerging post-graphene scenario, black phosphorus (BP) has emerged as a new 2D nanomaterial, which can be easily used for various biomedical applications, such as biosensing, drug delivery, and bioimaging.[13] The advantage of BP over other 2D materials is that BP demonstrates a wide range of band gap (0.3–2.0 eV) compared to the zero band gap of graphene, that can be tuned by adjusting the layer number. This optical property allows BP to demonstrate a broad absorption across ultraviolet, visible, and infrared light spectra and renders it an ideal candidate for biosensing.[13] Its ambipolar character-istic enables the detection of both positively and negatively charged biomolecules. It is thermodynamically stable at room temperature and non-toxic.[14] Owing to these unique physical, optical, and electrochemical properties, BP is considered an ideal candidate for different biomedical applications such as drug delivery, bioimaging, and biosensor.

Among various metal and metal oxides, Au and γ-Fe₂O₃ have been used repeatedly for various biomedical applications such as drug delivery, bioimaging and biosensors, due to their favorable physiochemical properties in cell system.[6,15] In addi-tion, several attempts have been made to hybridize these nanomaterials (Au and γ-Fe₂O₃) in order to achieve the result-ing synergistic properties.[16] In this regard, the synergistic property of Au and γ-Fe₂O₃ with BP will be of great interest to biomedical researchers as all of them have beneficial biomed-ical properties for biomedical applications. However, at first the

aDepartment of Chemistry and Chemistry Institute for Functional Materials, Pusan National University, Busan 46241, South Korea. E-mail: kwangsun.kim@pusan.ac.kr; Tel: +82-51-510-2241

bImmunotherapy Research Center, Korea Research Institute of Bioscience and Biotechnology, Daejeon, 34141, South Korea

biocompatibility of these nanocomposites for any potential use in cell system, need to be checked. It is also noted that the biocompatibility study of Au and γ-Fe$_2$O$_3$ immobilized on BP is still not established.

In this study, an efficient nanoplatform based on Au–γ-Fe$_2$O$_3$–BP nanocomposite was successfully synthesized through low-temperature solution synthesis process. Further, biocompatibility evaluation of the Au–γ-Fe$_2$O$_3$–BP nanocomposite by WST assays against human colon cancer cell lines (HCT-15) showed that the nanocomposite was non-toxic even at a concentration of $\sim$200 μg mL^{-1}. To the best of our knowledge, this is the first report on the synthesis of biocompatible nanocomposite Au–γ-Fe$_2$O$_3$–BP. This newly synthesized materials can be used in various biomedical applications such as drug delivery and biosensor.

2. Experimental section

2.1. Synthesis of γ-Fe$_2$O$_3$ (IO) nanoparticles

The process for the synthesis of γ-Fe$_2$O$_3$ (IO) was adopted from a previously reported work.[17] Initially, 2.5 g of iron(III) nitrate nonahydrate (Fe(NO$_3$)$_3$·9H$_2$O, Merck, $\geq$98%) was uniformly dispersed in 200 mL of de-ionized water with continuous stirring. In another beaker, 0.5 g of NaBH$_4$ was added in 25 mL of 3.5% NH$_4$OH solution. After that it was mixed with iron nitrate solution and the precursors were kept stirring at $\sim$100 °C for 2 h for the formation of γ-Fe$_2$O$_3$ (IO) nanoparticles. The solid materials were then separated out with the help of centrifugation. Finally, the products were washed with double distilled water and ethanol for several times by centrifugation and the samples were dried in an air oven at $\sim$60 °C for 3 h.

2.2. Synthesis of Au–γ-Fe$_2$O$_3$ (AIO) nanoparticles

The AIO nanoparticles were prepared as follows: 300 mg of IO nanoparticles were dispersed in 50 mL of deionized water. This mixture was ultrasonicated for 10 min and mixed with 3.0 mL of aqueous 0.05 M chloroauric acid (HAuCl$_4$·3H$_2$O, Au $\geq$ 49%) by stirring for 30 min, followed by the addition of 0.3 g of NaBH$_4$ in 10 mL of deionized water. The dispersed materials (precursors) were ultrasonicated for 15 min and stirred continuously for 2 h, resulting in the formation of AIO nanoparticles. The solid materials were further separated out by centrifugation, washed several times with deionized water and ethanol, and pelleted by centrifugation. Finally, the samples were dried in an air oven at $\sim$60 °C for 4 h.

2.3. Synthesis of black phosphorus nanosheets (BP NSs) and Au–γ-Fe$_2$O$_3$-black phosphorus (AIB) nanocomposite

2.3.1 Synthesis of BP NSs. BP NSs were prepared from bulk BP crystals by adopting a method previously reported by Ouyang *et al.*[18] with slight modification. Initially, 2.0 g of NaOH was added into 60 mL of *N*-methyl-2-pyrrolidone (NMP) and sonicated in water bath for 5 min. Then the supernatant was collected by centrifugation. Further, 25 mg of bulk BP crystals were added into the saturated NaOH solution mixed in NMP. The suspensions were ultrasonicated in an ice bath

ultrasonicator for 8 h. The bath temperature was consistently maintained under 20 °C during sonication. After completion of the exfoliation step, the dispersion was centrifuged at a rate of 2000 rpm for 15 min to remove the unexfoliated BP crystals. Finally, the BP NSs in the supernatant were collected by centrifugation (13 000 rpm for 10 min) and dispersed in water as a brown solution to store at 4 °C until further use.

2.3.2 Synthesis of AIB nanocomposite. Briefly, 2 mL (1.5 mg mL^{-1}) of as-prepared BP NSs were mixed with 200 mg of as-synthesized AIO NPs in 40 mL of deionized water and ultrasonicated for 10 min. The mixture was then continuously stirred for 6 h. Finally, the AIB nanocomposites were collected after centrifugation and vacuum drying at 60 °C for 6 h.

2.4. Characterization

The diffraction patterns of the IO, AIO, and AIB samples were obtained through X-ray diffraction (XRD) using an X-ray diffractometer (D8 Advance with DAVINCI design X-ray diffraction unit, Bruker) with nickel-filtered Cu K$_\alpha$ radiation source ($\lambda = 1.5406$ Å) in the 2θ range of 20–80°. Moreover, transmission electron microscopy (TEM; Bruker Nano GmbH) that employed carbon-coated 300 mesh Cu grids for the placement of IO, AIO, and AIB samples was employed for microstructural analysis. The AXIS Supra X-ray photoelectron spectroscopy (XPS) microprobe surface analysis system was used to assess the representative sample of AIB by scanning in the binding energy range of 200–1200 eV to determine the chemical state of elements. The C 1s peak position at 284.5 eV was used as the binding energy reference.

2.5. WST assay

HCT-15 cells (colon cancer) were purchased from the American Type Culture Collection (Manassas, VA, USA) and maintained in RPMI1640 with 10% of fetal bovine serum at 37 °C in 5% CO$_2$. The cell viability was determined through the colorimetric WST assay (Ez-Cytox; DoGenBio, Seoul, Korea). The cells were seeded into 96-well plates at a density of 4000 cells per well and incubated for 24 h. They were further incubated for 24 h or 48 h in the presence of IO/AIO/AIB samples with a concentration of 10–200 μg mL^{-1} in 0.1% dimethyl sulfoxide. The cells were then incubated with WST reagent (one-tenth of the medium volume), and the amount of formazan dye formed was determined by measuring the absorbance at 450 nm using a spectrophotometric microplate reader (BMG LABTECH GmbH, Ortenber, Germany). The morphology of HCT-15 cells treated with black phosphorus was imaged using a phase-contrast microscope (Leica DM IL LED; Leica, Wetzlar, Germany).

3. Results and discussion

3.1. Material properties

3.1.1 Phase structure. Fig. 1 displays the crystalline structure of the as-synthesized γ-Fe$_2$O$_3$ (IO), Au–γ-Fe$_2$O$_3$ (AIO), and Au–γ-Fe$_2$O$_3$–BP (AIB) determined by the XRD patterns. The XRD peaks of the as-synthesized IO, AIO, and AIB, observed at 30.18°, 35.60°, 43.34°, 53.71°, 57.25°, 62.97°, and 74.41° are indexed to
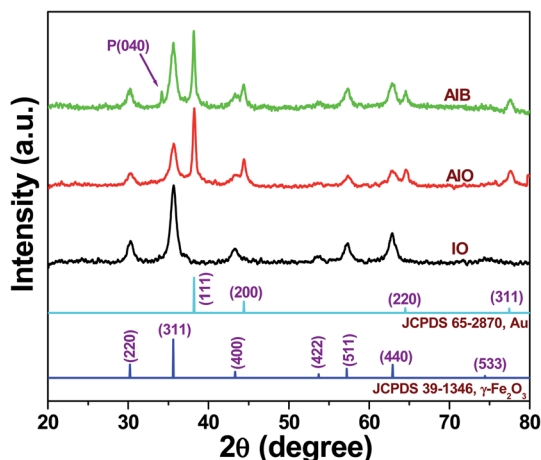
Fig. 1 X-ray diffraction patterns of IO, AIO and AIB samples.

the diffraction planes (220), (311), (400), (422), (511), (440), and (533), respectively, which entirely matches with the spinel structure γ-Fe_2O_3 [JCPDS 39-1346].[19] Moreover, some additional peaks were observed at 38.19°, 44.37°, 64.39°, and 77.46° with respect to AIO and AIB samples. These XRD peaks confirm the presence of cubic Au NPs [JCPDS 65-2870] with the corresponding crystal planes of (111), (200), (220), and (311).[20] The additional diffraction peak at 34.20° of the AIB sample corresponds to the (040) lattice plane of BP.[21] It also confirms that the exfoliated BP NSs still belong to the orthorhombic system, as there are no impurity peaks even after liquid ultrasonication. Therefore, the XRD result (Fig. 1) confirms the successful synthesis of the AIB sample.

The average crystallite size (D) of γ-Fe_2O_3 and Au were estimated along (311) crystal plane of γ-Fe_2O_3 and (111) crystal plane of Au, respectively by using Debye–Scherrer's eqn (1).

$$D = k\lambda/\beta \cos\theta, \qquad (1)$$

where, k is proportionality constant ($k = 0.89$), λ is the wavelength of X-ray (1.5406 Å), β is the FWHM (full width at half maximum) of the peak of maximum intensity in radians, θ is the diffraction angle and D is the crystallite size in nm.

The measured 'D' values of γ-Fe_2O_3 in IO, Au–γ-Fe_2O_3 (AIO), and Au–γ-Fe_2O_3-black phosphorus (AIB) samples were ~11.0 nm, ~11.0 nm, and ~11.0 nm, respectively. Likewise, the measured 'D' values of Au in AIO and AIB are ~19.0 nm. Thus, the crystallite size of γ-Fe_2O_3 in AIO and AIB, remained identical after the incorporation of Au and black phosphorus (BP), respectively. Therefore, no effect on the change of crystallite size of γ-Fe_2O_3 was found in AIO and AIB. The same result can be seen in Au nanoparticle size after the incorporation of BP in AIB sample where there is no change of Au nanoparticle in AIB sample.

3.1.2. Morphology and microstructure. Fig. 2a, b and c show the TEM images of IO, AIO, and AIB samples, respectively. The corresponding HRTEM images are also depicted in Fig. 2d, e and f for IO, AIO, and AIB, respectively. Shape information of the nanoparticles can be confirmed from TEM images of IO,

AIO, and AIB samples in Fig. 2 where the quasi-spherical nature of both (γ-Fe_2O_3 and Au) the nanoparticles can be seen. The incorporation of BP doesn't affect the shape of the nanoparticles. Additionally, Fig. 2c shows the TEM image of AIB nanocomposite, in which the Au and γ-Fe_2O_3 nanoparticles can be observed on the surface of BP NSs. The nearly transparent feature of BP due to its ultra-thin thickness is confirmed by the image (Fig. 2c). The presence of Au and γ-Fe_2O_3 nanoparticles is also confirmed through the results of high-resolution TEM (HRTEM; Fig. 2f), in which the distinct lattice fringes with an interplanar distance of 0.23 nm and 0.29 nm correspond to the (111) plane of Au[20] and (220) plane of γ-Fe_2O_3,[19] respectively. Therefore, TEM and HRTEM corroborate the XRD results (Fig. 1) and confirm the successful formation of the AIB nanocomposite. Additionally, the inset of Fig. 2c shows the energy-dispersive X-ray (TEM-EDX) spectral analysis of the AIB nanocomposite. The formation of γ-Fe_2O_3 is supported by the presence of Fe and O, as observed in the TEM-EDX spectrum. The existence of Au suggests the formation of Au nanoparticles in the AIB nanocomposite. Moreover, the presence of P reinforces the existence of BP and formation of the AIB nanocomposite. The additional existence of C and Cu observed in the TEM-EDX spectrum is attributed to the use of carbon-coated Cu grid for TEM measurements. The elemental mapping images of the AIB nanocomposite demonstrate good distributions of the O (Fig. 2i), Au (Fig. 2j), Fe (Fig. 2k), and P (Fig. 2l) elements. The successful formation of the AIB nanocomposite, which is confirmed by the XRD (Fig. 1) and TEM (Fig. 2) results, can be employed in future biomedical applications.

3.1.3. XPS results. The XPS measurements are generally used to evaluate the surface chemical composition and valence state of the elements. Fig. 3 shows the XPS result of the representative sample AIB, which demonstrates the binding energy signals of Fe 2p (Fig. 3a), Au 4f (Fig. 3b), and P 2p (Fig. 3c). The peaks observed at ~711 eV and ~724.6 eV in Fig. 3a can be assigned to the binding energy values of Fe $2p_{3/2}$ and Fe $2p_{1/2}$, respectively which are the characteristic peaks of Fe^{3+}. Furthermore, a satellite peak of Fe $2p_{3/2}$ is detected at ~719 eV, which is characteristic of Fe^{3+} in γ-Fe_2O_3.[22] The two peaks at ~83.75 eV and ~87.50 eV in Fig. 3b can be respectively assigned to the binding energy of Au $4f_{7/2}$ and Au $4f_{5/2}$, thereby confirming the formation of metallic Au in the nanocomposite.[20] Furthermore, the XPS spectrum shows the presence of P 2p (Fig. 3c) in the nanocomposite.[23] Therefore, the XPS results corroborate the XRD data and confirm the successful formation of the Au–γ-Fe_2O_3–BP (AIB) nanocomposite. The elemental analysis has also been made through XPS results. The analysis has been made from the peak areas of the corresponding XPS signal for Au and iron. The contents (at%) of Au and Fe are found to be ~7% and Zn ~93%, respectively.

3.2. *In vitro* cytotoxicity

The cell viability from the *in vitro* cellular cytotoxicity was assessed using the WST assay of HCT-15 cells (colon cancer) by varying the concentrations of the IO, AIO, and AIB samples. The corresponding results are shown in Fig. 4. Each bar graph in
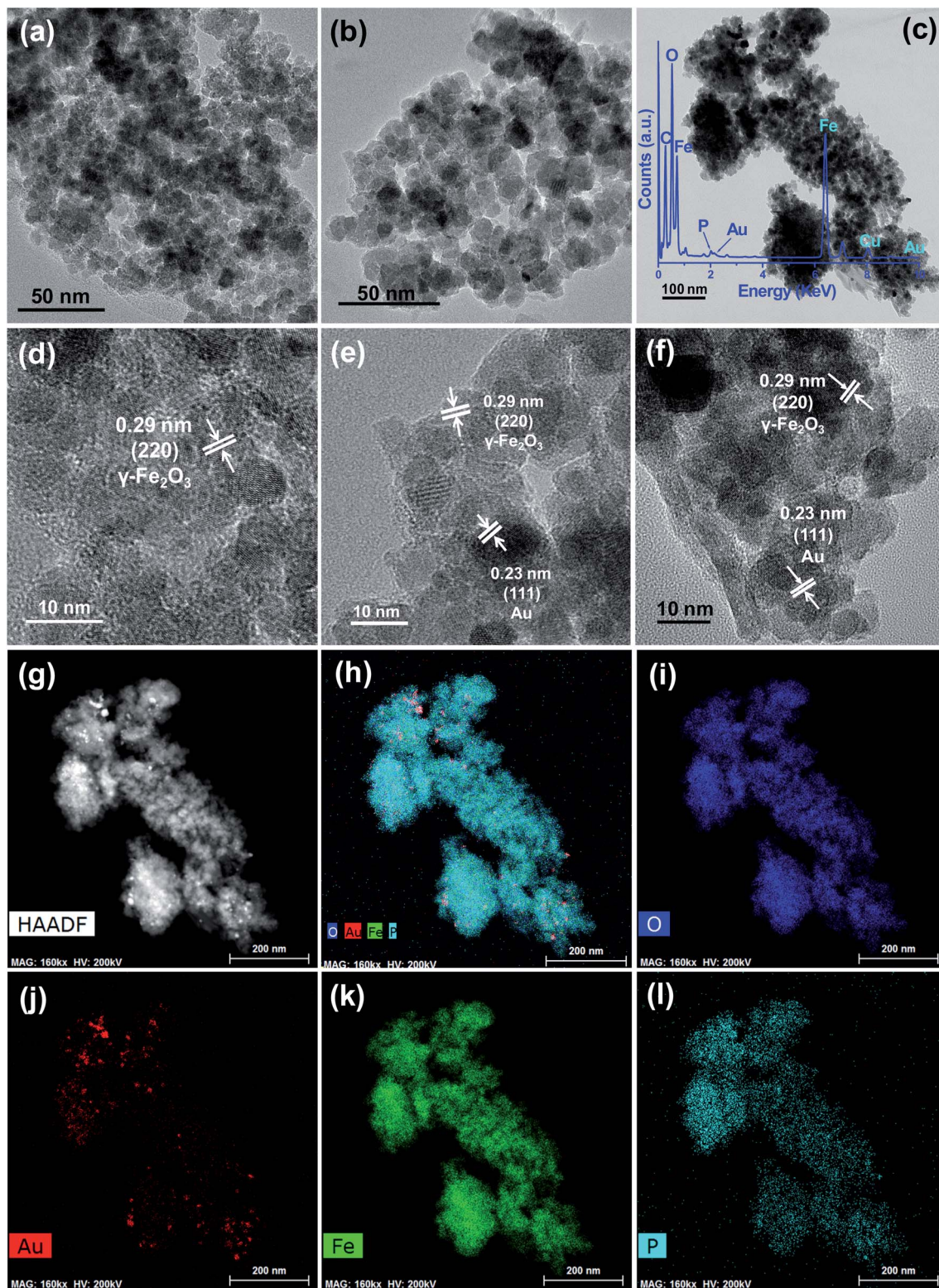
Fig. 2 TEM image of IO (a), AIO (b), AIB (c) and high-resolution TEM image of IO (d), AIO (e), AIB (f) sample. TEM-energy-dispersive X-ray spectrum (c inset), (g) HAADF image, and elemental mappings of (h) composite, (i) O, (j) Au, (k) Fe, and (l) P from AIB sample.

this figure represents the average of triplicate measurements. It can be clearly observed that the cell viability of the AIB nanocomposite is comparable to that of IO nanoparticles, and the

nanocomposite is non-toxic even after attaining the concentration of 200 μg mL^{-1}. Therefore, the use of BP with Au–γ-Fe$_2$O$_3$ nanoparticles shows relatively less harmful effects in
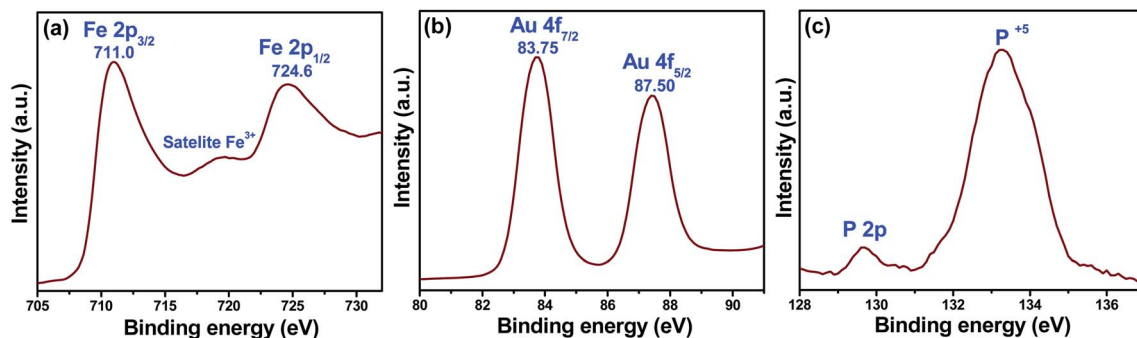
Fig. 3 X-ray photoelectron spectroscopy binding energy spectra of AIB (a) Fe 2p, (b) Au 4f, and (c) P 2p core levels.
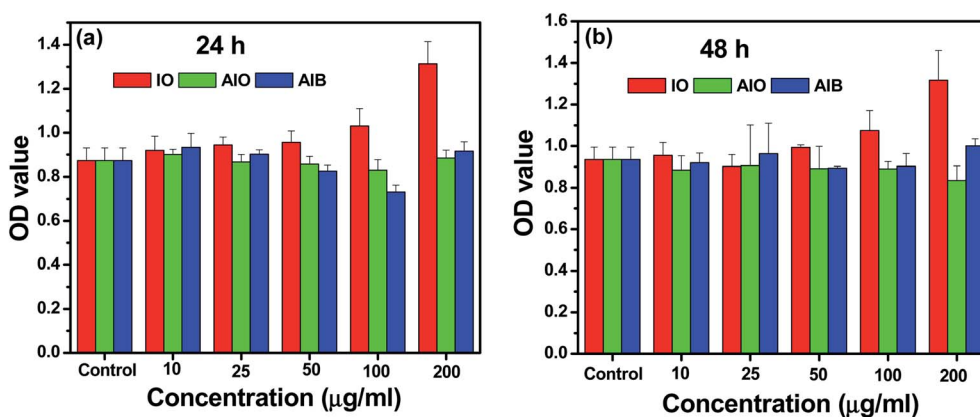

Fig. 4 Cell viability from *in vitro* cellular cytotoxicity, WST assay of HCT-15 cells (colon cancer) for IO, AIO, and AIB samples with varied concentrations. The error bars represent ±SD ($P < 0.05$).

human cells due to the biocompatible nature of BP. It is reasonable to state that the AIB nanocomposite is biocompatible and can be effective in various biomedical applications such as drug delivery.

4. Conclusions

In this study, we developed a novel synthesized nanocomposite of Au–γ-Fe$_2$O$_3$–BP, called AIB, by adopting low-temperature solution synthesis process. The method of preparation was simple, rapid, and easily reproducible. XRD, TEM, and XPS characterization techniques were used to evaluate the material properties of the samples. The synthesized nanocomposite showed excellent cell viability even at 200 μg mL^{-1} concentration. This cost-effective simple synthesized nanocomposite can be useful for a wide range of biomedical applications.

Conflicts of interest

The authors declare no competing financial interest.

Acknowledgements

References

1 S. Pattnaik, K. Swain and Z. Lin, *J. Mater. Chem. B*, 2016, **4**, 7813–7831.
2 C. Yang, H. Wei, L. Guan, J. Guo, Y. Wang, X. Yan, X. Zhang, S. Wei and Z. Guo, *J. Mater. Chem. A*, 2015, **3**, 14929–14941.
3 A. P. Subramanian, S. K. Jaganathan and E. Supriyanto, *RSC Adv.*, 2015, **5**, 72638–72652.
4 S. A. C. Carabineiro, N. Bogdanchikova, P. B. Tavares and J. L. Figueiredo, *RSC Adv.*, 2012, **2**, 2957–2965.
5 K. Li, Y. Lai, W. Zhang and L. Jin, *Talanta*, 2011, **84**(3), 607–613.
6 S. Sabale, P. Kandesar, V. Jadhav, R. Komorek, R. K. Motkuri and X.-Y. Yu, *Biomater. Sci.*, 2017, **5**, 2212–2225.
7 S. Palanisamy and Y.-M. Wang, *Dalton Trans.*, 2019, **48**, 9490–9515.
8 A. Naskar and K.-s. Kim, *Microb. Pathog.*, 2019, **137**, 103800.
9 M. Soleymaniha, M. -A. Shahbazi, A. R. Rafieerad, A. Maleki and A. Amiri, *Adv. Healthcare Mater.*, 2019, **8**, 1801137.
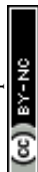
10 K. D. Patel, R. K. Singh and H.-W. Kim, *Mater. Horiz.*, 2019, **6**, 434–469.

11 M.-A. Shahbazi, L. Faghfouri, M. P. A. Ferreira, P. Figueiredo, H. Maleki, F. Sefat, J. Hirvonen and H. A. Santos, *Chem. Soc. Rev.*, 2020, **49**, 1253–1321.

12 Y.-P. Ho and K. W. Leong, *Nanoscale*, 2010, **2**(1), 60–68.

13 M. Luo, T. Fan, Y. Zhou, H. Zhang and L. Mei, *Adv. Funct. Mater.*, 2019, **29**(13), 1808306.

14 S. Anju, J. Ashtami and J. P. V. Mohanan, *Mater. Sci. Eng., C*, 2019, **97**, 978–993.

15 N. V. S. Vallabani and S. Singh, *3 Biotech*, 2018, **8**, 279.

16 F. Parnianchi, M. Nazari, J. Maleki and M. Mohebi, *Int. Nano Lett.*, 2018, **8**(4), 229–239.

17 Z. Heger, N. Cernei, I. Blazkova, P. Kopel, M. Masarik, O. Zitka, V. Adam and R. Kizek, *Chromatographia*, 2014, **77**, 1415–1423.

18 J. Ouyang, R.-Y. Liu, W. Chen, Z. Liu, Q. Xu, K. Zeng, L. Deng, L. Shen and Y.-N. Liu, *J. Mater. Chem. B*, 2018, **6**, 6302–6310.

19 A. Naskar, S. Bera, R. Bhattacharya, S. S. Roy and S. Jana, *Biointerface Res. Appl. Chem.*, 2018, **8**(6), 3751–3757.

20 A. Naskar, S. Bera, R. Bhattacharya, S. S. Roy and S. Jana, *J. Alloys Compd.*, 2018, **734**, 66–74.

21 J. Song, J. Wang, X. Lin, J. He, H. Liu, Y. Lei and Z. Chu, *ChemElectroChem*, 2017, **4**, 2373–2377.

22 J. A. Cuenca, K. Bugler, S. Taylor, D. Morgan, P. Williams, J. Bauer and A. Porch, *J. Phys.: Condens. Matter*, 2016, **28**, 106002.

23 R. Gusmão, Z. Sofer, D. Bouša and M. Pumera, *ACS Appl. Energy Mater.*, 2018, **1**, 503–509.